from the equation of Fischer and Seraphin[10,11]:

$$\delta R/R=\alpha(\phi,\epsilon_1,\epsilon_2)\delta\epsilon_1+\beta(\phi,\epsilon_1,\epsilon_2)\delta\epsilon_2, \quad (6)$$

where α and β are also functions of the polarization of the incident light when $\phi\neq 0$. It is obvious that the two terms of (6) might nearly cancel, even when the structure in $\delta\epsilon_1$ and $\delta\epsilon_2$ is pronounced, if α and β had proper magnitude and sign.

The measurements are consistent with the usual interpretation of the band structure in Au and Ag. The $L_{32}\rightarrow L_2'$ transition at 2.1 eV in Au and the hybrid interband transition and plasma resonance at 3.9 eV in Ag are clearly visible. Analysis of the $\delta\epsilon_1$ and $\delta\epsilon_2$ lineshapes obtained by this method should aid the study of other excitations, in these and other materials, whose identification from band theory may be less clear, since parabolic and saddle-point transitions give easily identified characteristic line shapes.

This theory assumes scalar ϵ_1, ϵ_2, $\delta\epsilon_1$, and $\delta\epsilon_2$. The obliquely incident beam is affected by components of the tensors $\delta\epsilon_1$ and $\delta\epsilon_2$ both along and perpendicular to the modulating field. This is not the case with normal-incidence measurements, where the electric vector of the light is always perpendicular to the applied electric field. The agreement of our calculated $\delta R/R$ spectra with those observed in normal-incidence experiments suggests that the anisotropy introduced is small. This may be due to the fact that, in a polycrystalline film, the crystal axes effectively assume all orientations with respect to the optical and applied fields. The tensor character of $\delta\epsilon_1$ and $\delta\epsilon_2$, contained in matrix elements which in turn depend on crystal orientation with respect to the modulating field,[12–14] may thus be masked in polycrystalline samples.

[10] B. O. Seraphin and N. Bottka, Phys. Rev. Letters **15**, 104 (1965).
[11] J. E. Fischer and B. O. Seraphin, Solid State Commun. **5**, 973 (1967).
[12] D. E. Aspnes, Phys. Rev. **147**, 544 (1966).
[13] D. E. Aspnes, Phys. Rev. **153**, 972 (1967).
[14] D. E. Aspnes, P. Handler, and D. F. Blossey, Phys. Rev. **166**, 921 (1968).

PHYSICAL REVIEW VOLUME 174, NUMBER 3 15 OCTOBER 1968

Magnetoacoustic Dispersion and Attenuation; Comparison of Experiment with the Free-Electron Theory*

A. G. BEATTIE
Sandia Laboratory, Albuquerque, New Mexico 87115
(Received 2 May 1968)

The Cohen-Harrison-Harrison formalism has been used to calculate longitudinal magnetoacoustic dispersion and attenuation curves in transverse fields for values of the parameter ql between 1.0 and 200 ($ql=\omega v_f\tau/v$). The results of this calculation show that as ql is decreased from the limiting case of $ql\gg 1$, the oscillations in the attenuation are damped out faster than the oscillations in the dispersion. Experimental data are given for both the attenuation and fractional velocity shift in aluminum and are shown to be in qualitative agreement with the theory. An examination of magnetoacoustic-attenuation data in potassium shows that the deviation of the attenuation minima from the positions predicted in the limit $ql\gg 1$ agrees quantitatively with theory.

INTRODUCTION

THEORETICAL treatments of the magnetoacoustic effect can be divided into those based upon the free-electron model of a metal and those which are designed to apply to a metal with an arbitrary Fermi surface. Both types of treatments are semiclassical in nature and both assume an isotropic electron relaxation time over the Fermi surface.

A comprehensive treatment of ultrasonic attenuation in real metals is given by Pippard.[1] He first considers the attenuation in the absence of a magnetic field and then applies the field. The effect of real metals on the attenuation is introduced by means of a deformation parameter. This parameter is a measure of how the local Fermi surface deforms when subjected to a strain. In the presence of an acoustic wave, this strain is produced by the electric field set up between the ions and electrons by the wave. It would appear that such a treatment, which can be used for arbitrarily shaped Fermi surfaces and which includes variations in the strength of the coupling between the electrons and the acoustic phonons, should be used in interpreting experimental magnetoacoustic data. However, when this is attempted, several inherent difficulties appear. One problem is that a determination of the shape of the attenuation curve involves evaluating many integrals over the Fermi surface. Thus, while one can predict the shape of the experimental curve if the Fermi surface is known, it is far more difficult to determine the

* Work supported by the U. S. Atomic Energy Commission.
[1] A. B. Pippard, Proc. Roy. Soc. (London) **257**, 165 (1960).

Fermi surface from the shape of the experimental curve. In addition, many of these integrals over the Fermi surface contain the deformation parameter. The form of this parameter is not well known and has been experimentally determined only partially for the noble metals.[2] While this parameter should, in principle, be calculable from a pseudopotential approach, this has not yet been done. In view of these difficulties, it appears that it might be preferable to use a theory based upon the free-electron model for a guide in interpreting experimental data.

The free-electron theory of magnetoacoustic attenuation was first correctly developed by Kjeldaas and Holstein.[3] Their treatment was aimed specifically at geometries associated with experimental work. In it, curves are given showing the variation in the shape of the attenuation curves as a function of the parameter ql (q is the acoustic wave number and l is the electron mean free path). Cohen, Harrison, and Harrison[4] (CHH) then developed a complete formalism for the magnetoacoustic attenuation. This formalism applies to all geometries of magnetic field direction and acoustic polarization vector and, in addition, holds for all values of ql. However, in their application of the formalism, they restricted themselves to the limiting case of $ql \gg 1$. Here it should be noted that Pippard's treatment gives the CHH results when applied to a free-electron gas. Subsequently, Shah and Meijer[5] used the CHH formalism to calculate attenuation curves for several values of ql. Flax and Trivisonno[6] have also determined the attenuation at several values of ql and, in addition, give series solutions which can be used to calculate the attenuation for arbitrary values of ql.

Magnetoacoustic-attenuation experiments, in which the necessary requirements of frequency and sample purity have been met, have shown oscillatory behavior similar to that predicted by the CHH theory. In general, the shapes of these attenuation curves are more complex than those predicted by CHH. This complexity arises from three main sources. They are differing phases for the oscillations because of departures of the orbit shapes from circles, more than one band of electrons giving rise to oscillations, and a background attenuation caused by a noncoherent sum of attenuations arising from all other orbits on the Fermi surface. The best agreement between the shapes of experimental and theoretical curves should be seen in the alkali metals because of their near-spherical Fermi surfaces. Such agreement is apparent in the experimental studies on potassium by Trivisonno, Said, and Pauer[7] and by Foster, Meijer, and Mielczarek.[8] Thus, to date, free-electron theory gives a good qualitative prediction of the behavior of the magnetoacoustic attenuation in potassium and appears to give generally correct qualitative predictions of the behavior of the attenuation in other metals.

In addition to the attenuation, one can also measure the acoustic dispersion caused by the magnetoacoustic effect. Rodriguez[9] has applied the CHH formalism to calculate the fractional velocity shift $\Delta v/v$. The calculation is restricted to the limiting case $ql \gg 1$ and in this limit shows that the functional dependence of the attenuation and velocity shift upon the magnetic field are the same. In an experimental investigation of the velocity shift in aluminum, Beattie and Uehling[10] (BU) found that for values of ql around 4 the velocity shift appeared to have a stronger set of oscillations than the attenuation for the same electron orbits. While aluminum is very free-electron-like in character, it does not have a spherical Fermi surface. This raised the question as to whether the free-electron theory applies to all metals having a free-electron character or only to those metals which have a spherical Fermi surface. It therefore appeared desirable to extend the calculation of the velocity shift to low values of ql in order to investigate the possible divergences between the functional dependence on the field of the dispersion and attenuation at small ql.

In this paper, the formalism of CHH is used to calculate both the fractional velocity shift and the attenuation for values of ql between 1 and 200. The calculation shows that for $ql < 20$ the functional dependences of the attenuation and dispersion diverge, with the dispersion showing a stronger oscillatory behavior than the attenuation at a given value of ql. In addition, new experimental data on aluminum are presented. The results show that the free-electron theory does apply remarkably well to free-electron metals with nonspherical Fermi surfaces. While the shapes of the experimental curves differ from those predicted because of the nonspherical surface, it appears that all behavior seen is qualitatively predicted by theory.

THEORY

In this section the theoretical development will be briefly sketched and the results presented. Details of the numerical calculation will be reserved for the Appendix. The approach is basically that of Rodriguez[8] in which the equation of motion of the ions is set up and solved for both the real and imaginary parts of the acoustic velocity. For simplicity, cubic symmetry is

[2] R. E. MacFarlane and J. A. Rayne, Phys. Rev. **162**, 532 (1967).
[3] T. Kjeldaas and T. D. Holstein, Phys. Rev. Letters **2**, 340 (1959).
[4] M. H. Cohen, M. J. Harrison, and W. A. Harrison, Phys. Rev. **117**, 937 (1960).
[5] B. P. Shah and P. H. E. Meijer, J. Acoust. Soc. Am. **36**, 327 (1964).
[6] L. Flax and J. Trivisonno, Phys. Letters **22**, 569 (1966).
[7] J. Trivisonno, M. S. Said, and L. A. Pauer, Phys. Rev. **147**, 518 (1966).
[8] H. J. Foster, P. H. E. Meijer, and E. V. Mielczarek, Phys. Rev. **139**, A1849 (1965).
[9] S. Rodriguez, Phys. Rev. **130**, 1778 (1963); **132**, 535 (1963).
[10] A. G. Beattie and E. H. Uehling, Phys. Rev. **148**, 657 (1966).

used. The oscillatory part of the result for both the attenuation and the dispersion will be valid for any system where a pure longitudinal wave is propagated. However the small transverse component present in any longitudinal wave propagating in a finite medium should not effect the results of the calculation. The calculation is also restricted to a magnetic field perpendicular to the direction of propagation.

Longitudinal plane waves are assumed traveling along the x axis with the form of $\exp i(\mathbf{q}\cdot\mathbf{x}-\omega t)$. The external field $\mathbf{B}_0$ is applied along the z axis. An equation of motion for the ions can be written

$$N_0M\ddot{\mathbf{r}}=C_l\nabla\nabla\cdot\mathbf{r}-C_t\nabla\times\nabla\times\mathbf{r}+Ne[\mathbf{E}+\dot{\mathbf{r}}\times(\mathbf{B}_0+\mathbf{B})]-Nm(\dot{\mathbf{r}}-\dot{\mathbf{s}})/\tau. \quad (1)$$

In this equation, the C's are the elastic constants of the bare lattice, N_0 is the number of ions per unit volume, M is the ion mass, $\mathbf{E}$ and $\mathbf{B}$ are the fields associated with the acoustic wave, $\mathbf{r}$ and $\mathbf{s}$ are the mean displacements of the ions and electrons, respectively, and τ is the mean electron relaxation time. The last term gives the momentum transfer per unit time from the electrons to the lattice. The term involving the magnetic field associated with the ion currents, B, can be dropped without introducing an appreciable error, and it can be shown using Maxwell's equations that the momentum-transfer term is about a factor of 10^{-10} the size of the third term on the right. For longitudinal motion, only the x component of Eq. (1) is necessary. This can be written

$$N_0M\omega^2r_x=C_lq^2r_x-NeE_x. \quad (2)$$

The problem is now reduced to determining E_x. The formalism of CHH can be used to calculate E_x in the following manner. The electric field is linearly related to the ion velocity, and this defines the tensor $\mathbf{W}$:

$$\mathbf{E}=N_0e\mathbf{W}\cdot\dot{\mathbf{r}}/\sigma_0, \quad (3)$$

from which

$$E_x=(-i\omega N_0er_x/\sigma_0)W_{xx}. \quad (4)$$

From CHH we can write W_{xx} in terms of the conductivity tensor $\boldsymbol{\sigma}$ as

$$W_{xx}=1-i\Delta\sigma_0-\sigma_0\sigma_{yy}/(\sigma_{xx}\sigma_{yy}-\sigma_{xy}^2). \quad (5)$$

To obtain this result, terms involving $\beta=-\omega/\mu v^2\sigma_0$ have been omitted. For acoustic frequencies less than 1 GHz, and for pure samples with $\tau\geq10^{-11}$ sec, β is less than 10^{-3}, making this a reasonable approximation. Here σ_0 is the dc conductivity $Ne^2\tau/m$, and $\Delta=\omega\tau v_f^2/3\sigma_0v^2(1-i\omega\tau)$. Substituting the CHH expressions for the components of $\boldsymbol{\sigma}$ into Eq. (5) gives the final expression

$$v^2=\frac{\omega^2}{q^2}=\frac{C_l}{N_0M}+\frac{mv_f^2}{3M(1+\omega^2\tau^2)}+\frac{mv_f^2\omega^2\tau^2}{3M}f(B_0,k,ql)+i\frac{mv_f^2\omega\tau}{3M}g(B_0,k,ql), \quad (6)$$

and from Eq. (6) the fractional velocity shift and attenuation can be written

$$\Delta v/v=(E_f\omega^2\tau^2/3Mv^2)f(B_0,k,ql),\qquad \alpha=(2E_f\omega^2\tau/3Mv^3)g(B_0,k,ql). \quad (7)$$

The magnetoacoustic oscillations arising from the geometric resonances are contained in the oscillatory functions f and g. In the limit of $ql\gg1$ these two functions differ only by a constant and therefore have the same functional dependence upon the magnetic field. However, as ql approaches unity, the oscillatory behavior of g damps out faster than that of f. Figures 1–3 are plots of the fractional velocity shift and attenuation as a function of the parameter qv_f/ω_c for several values of ql. In this calculation, all terms in $\omega^2\tau^2$ have been kept. From the definition of ql we can write $\omega\tau=(v/v_f)ql$. For the purpose of the calculation we have set $v/v_f=300$, which is very close to the correct value for longitudinal waves in both aluminum and copper.

EXPERIMENTAL APPARATUS

The design of the experiment is based on the continuous wave phase comparison technique described in BU. The apparatus has been considerably modified

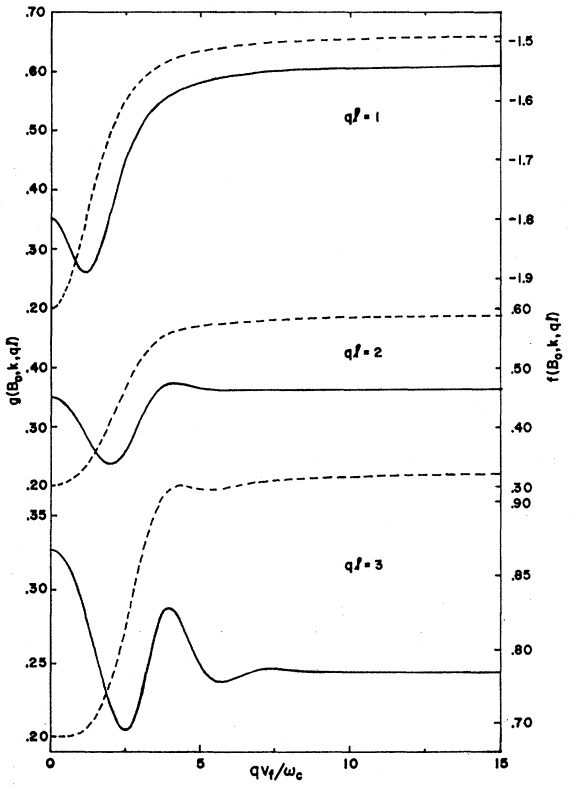

FIG. 1. Theoretical curves for the functions $f(B_0,k,ql)$ and $g(B_0,k,ql)$ for values of ql of 1.0, 2.0, and 3.0. The function f gives the behavior of the fractional velocity shift, and g gives the attenuation. Throughout the figures, the fractional velocity shift is a solid curve and the attenuation is dashed.

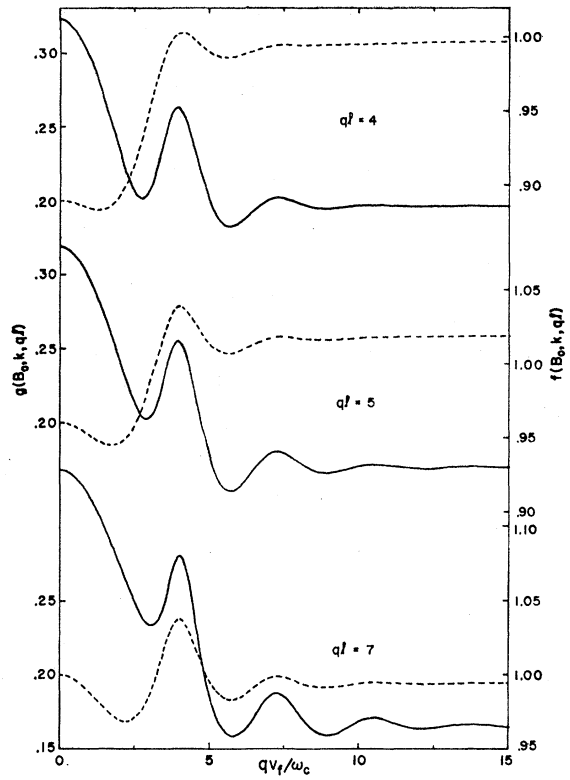

FIG. 2. Theoretical curves of f and g for values of ql of 4.0, 5.0, and 7.0.

from that used in BU to allow for the continuous recording of the phase shift and attenuation as a function of magnetic field. A block diagram of the apparatus is given in Fig. 4. The rf generator is frequency-stabilized to a few parts in 10^7 by the synchronizer. The fine tuning control of the synchronizer and the counter allow the frequency to be set to any desired value to within about ± 5 Hz at 50 MHz. The use of the Hewlett-Packard 8405A vector voltmeter to measure both phase and amplitude allows the continuous recording of both attenuation and phase shift as a function of magnetic field. The field is measured by tapping the output of a 0.01% Rawson gaussmeter used in the field control circuits of a Harvey-Wells magnet.

Ten MHz X-cut quartz transducers were used. The bonding agent was Dow Corning 200 fluid of viscosity 200 000 centistokes. It was noted in pulse experiments that this bonding material exhibited rather anomalous acoustic behavior above the solidifing temperature. However, its performance at nitrogen and helium temperatures was satisfactory. The sample holder was a modification of the one described in BU. The tin casting around the sample was eliminated and a conducting paint was used to ground the sample and improve the shielding. This modification did eliminate the degradation of the sample because of temperature cycling but did not improve the electrical characteristics of the system.

The sample was a right circular cylinder, cut by spark erosion from a zone-refined ingot of aluminum.[11] It was oriented by Laue back reflection and cut with a [110] crystal axis along the cylinder axis. The cylinder end faces were spark-planed flat and to within $\frac{1}{2}°$ of (110) planes. Final planing of the faces was done on the lowest range (position 7) of a Servomet spark cutter and faces were then very lightly polished to remove the carbon. The residual resistivity ratio of the sample ($R_{295}/R_{4.0}$) was determined by the eddy-current-decay method[12] to be $5500\pm 10\%$. Measurements of the ratio were made at the beginning and end of the experiment and no change was seen. The average electron relaxation time corresponding to this ratio is 3.8×10^{-11} sec. All data were taken at 2.0°K. This eliminated the noise arising from bubble formation against the faces of the transducers. The sample conductivity appeared to be impurity limited and no change in ql was detected between 4.0 and 2.0°K.

The phase noise in the vector voltmeter is about $\pm 0.1°$ for high signal amplitudes. For low signal ampli-

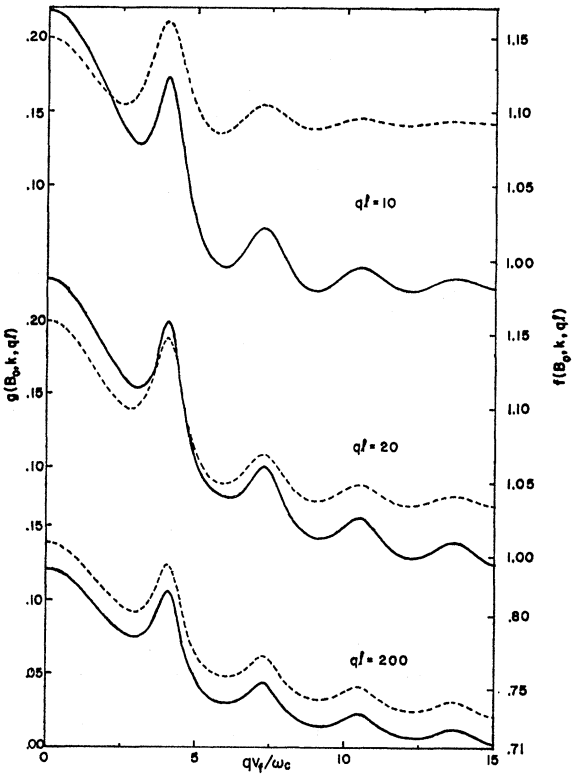

FIG. 3. Theoretical curves of f and g for values of ql of 10, 20, and 200.

[11] The sample was cut from an ingot of Cominco 69 grade aluminum.

[12] C. P. Bean, R. W. DeBlois, and L. B. Nesbitt, J. Appl. Phys. 30, 1976 (1959).

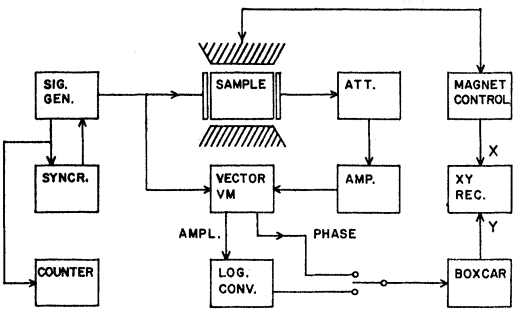

FIG. 4. Block diagram of the experimental apparatus.

tudes into the voltmeter, the noise level increased. It was found that the noise was essentially white. This allowed a substantial increase in the signal-to-noise level by running the output of the vector voltmeter through an amplifier with a long time constant. A boxcar integrator used in the continuous mode with time constants from 1 to 10 sec allowed a phase resolution of 0.01°. Neglecting any experimental difficulties, the fractional velocity shift is $\Delta v/v = v\Delta\theta/(360Lv)$, where L is the sample length and $\Delta\theta$ is in degrees. For an aluminum sample with a length of 1 cm at a frequency of 50 MHz, this gives a resolution in the fractional velocity shift of better than 0.4 ppm. The magnetic field can be read off the XY recorder to an accuracy of ± 5 G.

The signal amplitude was converted to an attenuation by running the output of the vector voltmeter through a logarithmic converter. The attenuation could be calibrated by means of the turret attenuator in the receiving line of the system. For this calibration, the field was held constant at the point of lowest attenuation and the attenuator changed in appropriate steps until the received signal amplitude was smaller than the signal had been at the point of highest attenuation. Each plot of the attenuation was calibrated in this manner. At the frequencies reported here, the change in the voltage standing wave ratio between the individual attenuator pads was negligible and the difference in phase shift across the individual pads was less than 0.5° for the worst pair. The estimated possible error in the attenuation measurement is less than ± 0.05 dB.

RESULTS AND DISCUSSION

The experimental geometry for the data reported here had a longitudinal acoustic wave propagating down a [110] crystal axis with the magnetic field lying along a $[1\bar{1}0]$ axis. This field direction picks a band of orbits, roughly hexagonal in shape, lying on the second-zone hole surface of aluminum. The sides of the hexagon are concave and this radical departure from a circular orbit gives rise to magnetoacoustic oscillations with a phase, in $1/\lambda H$, quite different from that predicted by free-electron theory. This difference in phase plus the addition of a second weaker oscillation, seen by Kamm and Bohm,[13] makes any detailed comparison of the experimental curve shape with theory impossible. In general, all field orientations in aluminum will give oscillatory patterns composed of oscillations with several periods and different phases. The field direction selected gives one of the strongest and cleanest sets of oscillations. An example of these oscillations in the attenuation is given in Fig. 5. This curve was obtained by standard pulse-echo techniques at 140 MHz. The sample was a disk sliced from the end of the cylinder used in the velocity-shift experiments. The distortion in the relative heights of the peaks is caused by the presence of the low-frequency oscillation.

Experimental curves for both the attenuation and fractional velocity shift are presented for 30 MHz in Fig. 6(a) and for 50 MHz in Fig. 7(a). From the estimated electron relaxation time, the values of ql for these curves were calculated to be 2.3 and 3.7, with an uncertainty of $\pm 10\%$. In Figs. 6(b) and 7(b) the theoretical functions $f(B_0,k,ql)$ and $g(B_0,k,ql)$ are plotted for these values of ql. These values of ql are obtained from the eddy-current-decay measurement of the electron relaxation time. This measurement was taken with the field parallel to a [110] axis so as to have the same distribution of electron orbits on the Fermi surface as was present in the experiment. The eddy-current-decay method will pick out the longest relaxation time present in the metal for any sizable band of orbits. For this field direction, the largest band of orbits is the one giving rise to the magnetoacoustic oscillations. Therefore these values are thought to be correct to within experimental accuracy.

The exact shapes of the fractional velocity shift curves were sensitive to small changes in frequency. This sensitivity arises from two different types of ex-

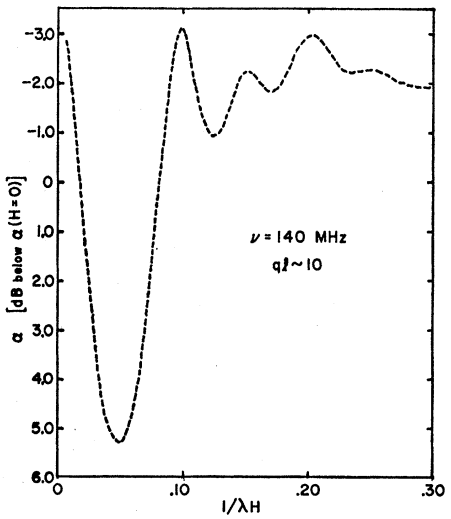

FIG. 5. Magnetoacoustic attenuation curve taken by the pulse-echo method at 140 MHz. The ql for this curve is about 10.

[13] G. N. Kamm and H. V. Bohm, Phys. Rev. 131, 111 (1963).

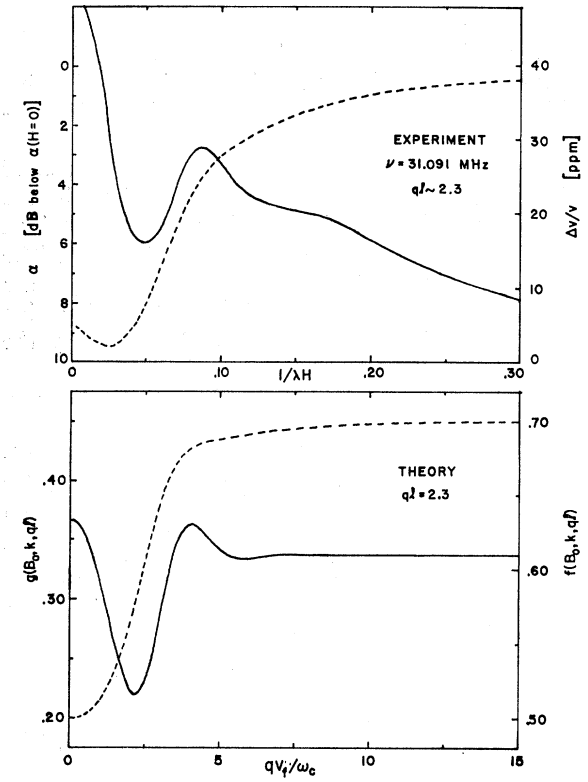

FIG. 6. (a) Experimental curves for the fractional velocity shift in aluminum taken at 31.091 MHz. The approximate ql is 2.3. (b) Theoretical curves of f and g for a ql of 2.3.

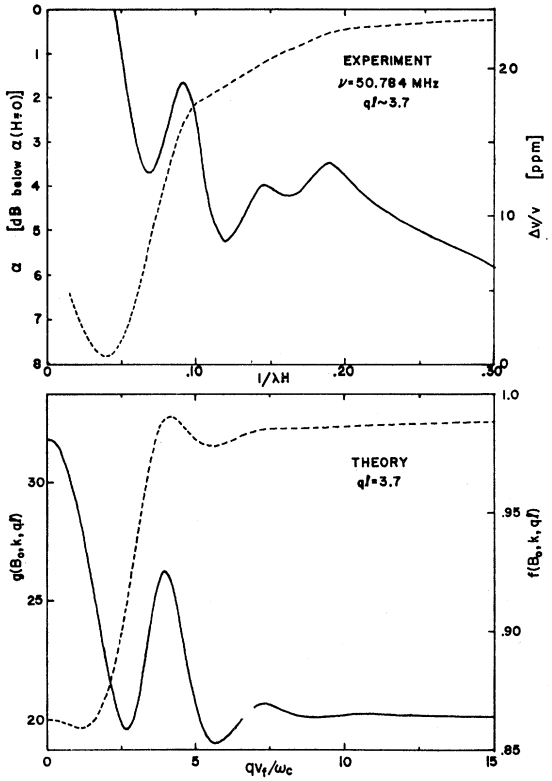

FIG. 7. (a) Experimental curves taken at 50.784 MHz. The approximate value of ql is 3.7. (b) Theoretical curves of f and g for a ql of 3.7.

perimental difficulties. These are rf leakage from the transmitting line to the receiving line and the occurrence of standing waves in the sample. Both will cause any changes in the signal amplitude to be reflected in the measured phase shift. This will occur at most frequencies. However, there are narrow frequency bands, spaced at intervals of $\Delta\nu=v/2L$ ($\Delta\nu=330$ kHz for this sample), where the phase shift is caused primarily by the velocity shift. The width of these bands varies from about 20 kHz for interference caused primarily by leakage to 10 Hz for interference caused by a large-amplitude standing wave. The interference by the standing waves rapidly decreased as the frequency, and thus the attenuation, was raised, while the interference from leakage increased with an increase in frequency. Inside the bands the curve shapes are still somewhat distorted by the attenuation changes. Thus care had to be used in choosing the exact frequency. The criterion used was to find a frequency where the shapes of the curves resembled those predicted by theory and the shifts had the correct sign, i.e., corresponded to an increase in the velocity. For the 50-MHz curve, the frequency was set to maximize the resemblance between the shape of the oscillations and the shape of the attenuation curve shown in Fig. 5. The frequency-dependent distortions in the curve shapes appeared to arise almost completely from rf leakage at 50 MHz. At 30 MHz, these distortions appeared to be due to both rf leakage and the presence of standing waves. While both types of interference are periodic in the same frequency increment, they are not necessarily in phase. Probably because of this, distortions in the 30-MHz curve were larger and more difficult to eliminate. Attempts to take phase-shift curves at 10 MHz were also made. Here the leakage was low and standing waves appeared to cause most of the distortion. Unfortunately, the phase shifts were so violently frequency-dependent that the resulting curves could not be interpreted with any confidence. It did appear that at a precise frequency, set to within ± 10 Hz, the phase-shift curves had the approximate shape predicted by theory for a ql of 1. This behavior is contrasted to the 30- and 50-MHz data, where the curves had a recognizable, although distorted, shape over a frequency increment of about 20 kHz. In view of this, no 10-MHz data are presented since it is thought that the curve may well have been due to a fortuitous distortion and not caused by a velocity shift. The shapes of the attenuation curves, in contrast to those of the velocity shift, were independent of small changes in frequency. However, they did appear to be magnified by the experimental interferences. It is estimated that the attenuation at 50

MHz is about 25% too large while the 30-MHz attenuation may be 50–75% too large. There was no sign of any distortion other than magnification.

The distortions of the experimental curves caused by the nonspherical Fermi surface prevents any detailed comparison of the experimental and theoretical curve shapes. However, the changes in the shapes of the curves as ql changes can be compared. Free-electron theory predicts that as ql is reduced from the limit $ql \gg 1$, the oscillations in the attenuation curve will be damped out faster than the oscillations in the fractional velocity shift. Figures 6(a) and 7(a) show exactly this type of behavior. The number and strength of the experimental oscillations for both the velocity and attenuation at a given value of ql are in remarkable agreement with theory. While only data for the field parallel to a $[1\bar{1}0]$ axis are presented, other field orientations in the (110) plane perpendicular to the direction of propagation were investigated. All showed the same relative oscillatory behavior between the attenuation and velocity shift.

A comparison of the amplitudes of the fractional velocity shift with those predicted by theory is complicated by both the nonspherical Fermi surface and the experimental distortions. The best point of comparison is the magnitude of the shift between the first minimum and the first maximum. The theoretical size of this shift for the 30-MHz curve is 2.0 ppm and the experimental value is 13 ppm. For the 50-MHz curve, the theoretical value[14] is 3.1 ppm and the experimental value is 6.2 ppm. This agreement is not bad, considering the large-frequency dependence of the experimental values. For the 30-MHz curve, a frequency change of 2 kHz reduced the experimental shift to 6.5 ppm and a change of 10 kHz eliminated the oscillation completely, giving a curve shape similar to the attenuation curve. For the 50-MHz curve, a change of 3 kHz reduced the shift to 0.2 ppm while a change of 2 kHz in the other direction increased the shift to 11.9 ppm. At the present state of the art, it does not appear possible to obtain much more accurate amplitudes for the fractional velocity shifts than are presented here. The best that can be said is that experiment and theory appear to agree within a factor of 2 for the amplitude of the fractional velocity shift.

The ideal metal for a comparison of the experimental and theoretical curve shapes is potassium. Since the shape of the Fermi surface is spherical[15] to within a few parts in 10^3, the experimental curves should correspond almost exactly to those predicted by theory. One of the best tests of the theory would be to compare the positions of the first minima in the attenuation. The

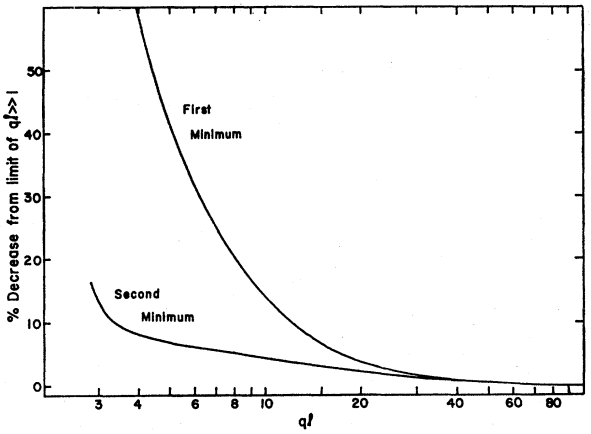

FIG. 8. Theoretical positions of the first and second minima in the attenuation as a function of ql. The positions are given as the percent deviation from their position in qv_f/ω_c in the limit $ql \gg 1$.

theory predicts that these minima will move to lower values of $1/\lambda H$ as ql decreases. Figure 8 is a plot of the predicted percentage decrease in $1/\lambda H$ as a function of ql for the first and second minima. The decrease is with respect to the position of the minima in the limit of $ql \gg 1$. Figure 9 is a plot of the positions of the minima of one experimental run in potassium. The data are from Trivisonno *et al.*[6] for their crystal number IV. Since no value for ql was given with these data, a value corresponding to the shift of the first minima was used. This gave a ql of 9. The uncertainty in the absolute accuracy of the data was given as about 4% but the internal consistency of the data was estimated to be better than this. It should be noted that the relative positions of the first two minima (which can be determined with higher accuracy than the others) are almost exactly those predicted by theory while the deviations of the positions of the other minima from theory are well within experimental error. Foster *et al.*[7] plot a similar curve for the deviations of the positions of the minima in potassium. The shape of this curve is not in

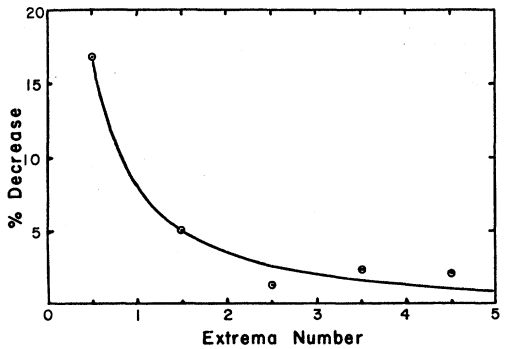

FIG. 9. Comparison of the theoretical positions of the attenuation minima with experimental data for potassium. The value of ql is taken to be 9.0. The experimental points are taken from Trivisonno *et al.* (Ref. 7).

[14] While the coefficient of the fractional velocity shift scales as q^2l^2, the difference in $f(B_0,k,ql)$ between the first minimum and the first maximum decreases as ql increases, especially at small values of ql. Therefore, this difference scales at a rate slower than q^2l^2.

[15] D. Shoenberg and P. J. Stiles, Proc. Roy. Soc. (London) **281**, 62 (1964).

good agreement with that predicted by theory. However, they describe the curve as being an average of their experimental values. If this average, as seems likely, was taken over several values of ql, then no comparison with theory is possible.

CONCLUSIONS

Free-electron theory for the magnetoacoustic effect predicts that the oscillations in the attenuation will damp out faster than oscillations in the fractional velocity shift when ql is decreased. This behavior is seen experimentally in aluminum. A comparison of the amplitude of the fractional velocity shift with the theoretical prediction shows agreement to within a factor of 2. Considering the experimental uncertainty and the nonspherical Fermi surface, this agreement seems good.

The distortion in the experimental curve shapes caused by the nonspherical Fermi surface prevents any comparison of the relative positions of the attenuation minima in aluminum with theory. When the positions of the attenuation minima for data taken in potassium are compared with theory, the agreement appears excellent.

It can be concluded that free-electron theory gives good quantitative predictions for the magnetoacoustic effect for metals with a spherical Fermi surface. For free-electron-like metals with nonspherical Fermi surfaces, the theory gives correct qualitative predictions for the magnetoacoustic effect. It is doubtful that the predictions of the theory will be in more than crude qualitative agreement with magnetoacoustic effects in non-free-electron-like metals. The magnetoacoustic effect in such metals can be expected to have large contributions from both deformation effects, as considered by Pippard, and anisotropic relaxation times.

ACKNOWLEDGMENTS

The author would like to thank Dr. H. B. Silsbee for much of the development of the theoretical approach presented here. He would like to thank Dr. E. A. Uehling for many valuable discussions and Dr. B. Morosin for aid in the programming of the calculation. The technical assistance of James Thomas is gratefully acknowledged.

APPENDIX

To calculate the function $f(B_0,k,ql)$, the components of $\boldsymbol{\sigma}$, σ_{xx}, σ_{xy}, and σ_{yy} must be obtained in series form with the real and imaginary parts separated. Series forms for these components, which are exact within the limits of the model, are given in CHH by Eqs. (4.1). The algebraic manipulation of these expressions is simplified by the relations $g_n(X)=g_{-n}(X)$, $g_n'(X)=g_{-n}'(X)$, and $S_n(X)=S_{-n}(X)$. Three algebraic expressions appear several times in each of the components. They are

$$D=1+2n^2\omega_c^2\tau^2+2\omega^2\tau^2+(n^2\omega_c^2\tau^2-\omega^2\tau^2)^2,$$
$$Y=(1+n^2\omega_c^2\tau^2+\omega^2\tau^2)/D,$$
$$Z=(1-n^2\omega_c^2\tau^2+\omega^2\tau^2)/D.$$

The components of σ can be written

$$\sigma_{xx}=(3\sigma_0/q^2l^2)(A-i\omega\tau B),\quad \sigma_{xy}=(3\sigma_0/2ql)(S-i\omega\tau U),$$
$$\sigma_{yy}=3\sigma_0(L+i\omega\tau Q),$$

where we define

$$A=1-g_0(x)-2(1-\omega^2\tau^2)\sum_{n=1}^{\infty}Yg_n(x)-4\omega^2\tau^2\sum_{n=1}^{\infty}Zg_n(x),$$

$$B=1-g_0(x)-4\sum_{n=1}^{\infty}Yg_n(x)+2(1-\omega^2\tau^2)\sum_{n=1}^{\infty}Zg_n(x),$$

$$S=g_0'(x)+Z\sum_{n=1}^{\infty}Yg_n'(x)+2\omega^2\tau^2\sum_{n=1}^{\infty}Zg_n'(x),$$

$$U=2\sum_{n=1}^{\infty}Yg_n'(x)-2\sum_{n=1}^{\infty}Zg_n'(x),$$

$$L=\frac{S_0(x)}{1+\omega^2\tau^2}+2\sum_{n=1}^{\infty}YS_n(x),$$

$$Q=\frac{S_0(x)}{1+\omega^2\tau^2}+2\sum_{n=1}^{\infty}ZS_n(x).$$

Then, using the relations

$$P=AL+\omega^2\tau^2BQ+\tfrac{1}{4}(S^2-\omega^2\tau^2U^2),$$
$$R=AQ-BL-\tfrac{1}{2}SU,$$

one can write the desired functions as

$$f(B_0,k,ql)=(PQ-LR)/(P^2+\omega^2\tau^2R^2),$$
$$g(B_0,k,ql)=\frac{LP+\omega^2\tau^2QR}{P^2+\omega^2\tau^2R^2}-\frac{1}{1+\omega^2\tau^2}-\frac{3}{q^2l^2}.$$

The computer program followed this algebra. The functions $g_n(X)$, $g_n'(X)$, and $S_n(X)$ were calculated from Eqs. (A1), (A2), and (A5) in CHH. For each of these functions, 80 terms in the series were retained to ensure convergence. It was found that for values of X up to 15 (where $X=qv_f/\omega_c$), $g_n(X)$, $g_n'(X)$, and $S_n(X)$ were essentially zero for n greater than 20. Therefore the sums $\sum_{n=1}^{\infty}Yg_n(X)$, etc., were truncated at 20 terms. From the definition of X one can write $\omega_c\tau=ql/X$ and, as was mentioned in the theory section, $\omega\tau=ql/300$.